Laboratory Study on Inclined Dense Jets in Perpendicular Cross-flow

Mostafa Taherian[1,*], Seyed Ahmad Reza Saeidi Hosseini[1], Abdolmajid Mohammadian[1], Simone Ferrari[2], Philip J. W. Roberts[3]

[1] Department of Civil Engineering, University of Ottawa, 75 Laurier Ave E, Ottawa, ON K1N 6N5, Canada

[2] Department of Civil-Environmental Engineering and Architecture (DICAAR), University of Cagliari, , Via Marengo, 2, 09123, Cagliari, Italy

[3] School of Civil and Environmental Engineering, Georgia Institute of Technology, Atlanta, GA 30332, USA

Abstract

To lessen the marine ecological footprint of dense effluents in the discharge regions, information regarding the influences of ambient currents and discharge characteristics on the outfall performance is essential. The mixing and transport behavior under the combined effects of discharge inclinations and flowing currents' strength for the desalination outfalls have remained unknown questions that should be addressed. For this purpose, a series of laser-induced fluorescence (LIF) experimental tests are applied for the measurement of 3D jet trajectory and concentration distribution of the submerged inclined dense jets while interacting with perpendicular cross-flows. Then, the influences of different discharge angles (30°, 45°, and 60°) and various cross-flow based Froude numbers ($u_rF = \frac{u_a}{u_0} \times \frac{u_0}{\sqrt{g_0' D}}$) within the range of critical current dictated regime are studied on the mixing level, and corresponding empirical equations are presented. The findings show that more than 50% and 2%0 dilutions can be achieved by deploying the jet of 60° compared to the 30° and 45° jets, respectively, due to the longer trajectory and more expansion of 60° jets. The positive impact of u_rF augmentation on the major flow parameters is also demonstrated. Accordingly, the presented outcomes provide valuable insights into the efficient design of inclined dense outfall discharges in coastal settings.

Keywords: Inclined buoyant jets; Jet in cross-flow; Submerged dense discharges; Laser-induced fluorescence; Dilution performance

[*] Corresponding author.
E-mail address: mtahe039@uottawa.ca (M. Taherian)

1 Introduction

Freshwater scarcity and security, which can be ascribed to population and economic growth, alteration of socioeconomic consumption patterns and living standards, and enlargement of irrigated agricultural industries, are becoming a critical concern on a worldwide scale [1,2]. As a sustainable supply remedy for clean water, the capacity of seawater reverse osmosis (SWRO) desalination technologies needs to expand [3–5]. This in turn increases the disposal of hypersaline by-products into the source oceanic environments. The SWRO brine effluents have a higher density compared to the receiving ambient waters, which leads them to sink to the seafloor and thus diminishes the quality of water and endangers the endemic benthic biota [6–10]. As a result, strict regulatory criteria are considered and required to be followed, particularly in terms of salinity limit and its impact distance from the brine disposal point, to reduce the relevant marine ecological detriment [2,8,11,12].

The widely accepted approach for safely discharging the brine effluents is to employ offshore diffuser structures. These diffusers should be designed in a way that the brine effluents be able to quickly become diluted to the level of near-background in order to minimize their environmental effects. This can be beneficially obtained by discharging the effluents through submerged turbulent buoyant jets at upward angles and high velocities containing both buoyancy and momentum fluxes [13–15]. For presenting an optimal design of turbulent buoyant jets, the influence of a number of factors should be investigated including the jet discharge configuration and ambient hydrodynamic forcing functions [11].

Regarding the discharge configuration, buoyant jets can be employed in the forms of inclined jets at an angle range of 0° to 90°, horizontal or vertical ones. In most situations, applying inclined jets offer more preferable results compared to the other configurations because of benefiting a horizontal momentum component [2,13,16,17]. Specifically, in case of releasing into shallow waters and close to the shoreline regions inclined dense jets are desirable to prevent impacting the water surface and thereby impairing dilution [18,19]. Regarding the ambient hydrodynamic characteristics, buoyant jets can be released into stationary and dynamic waters. The coastal settings which are representative of realistic conditions are rarely stationary and mainly predominated by flowing currents, turbulence, and shear [20,21]. This interplay with the ambient non-stationary environment not only makes the prediction of jet flow behavior essential but also more challenging.

As the basis for the design of dense outfalls, several studies have mainly targeted the discharge behavior into stationary water bodies in order to realize the optimal discharge angle

since the 1970s. In one of the earliest attempts, Zeitoun et al. [22] examined the dilution amounts for different inclinations using a point-based conductivity technique and introduced 60° as the best option in terms of having the longest trajectory and highest dilution compared to 30°, 45°, and 90°. Roberts et al. [13] also studied the dilution performance of the 60° discharge using a similar technique and provided more detailed measurements for this inclined angle. Further investigation on the inclination effects of dense jets' behavior was carried out by Kikkert et al. [23] using a light attenuation (LA) technique, and the dilution performance at the terminal point of jet trajectory was reported almost similar for the angles of 15°-60° while return point dilution was slightly higher for the 60°. Later, Jirka [24] questioned the de facto standard of 60° discharge angle by conducting an analytical study and stated that the 45° dense jet had a little higher terminal rise dilution. Papakonstantis et al. [25,26] and Lai and Lee [27] argued that the dilution performance was almost insensitive for the range of discharge angle 45°-75° using a conductivity technique and 38°-60° using a laser induced-fluorescence (LIF) technique, respectively. In addition, Oliver et al. [28] challenged the results of Jirka's study [24] and presented a significant impact of discharge angle on the return point dilution with about twofold dilution amount for 60° compared to 30°. Abessi and Roberts [16] also applied LIF techniques and presented a narrow variation in the dilution performance for the nozzle angles over 45°-65°.

In comparison, very limited studies have been conducted on the inclined dense discharges into dynamic water bodies although this scenario typifies a closer representative condition of the coastal environment [20,21,29]. It can add further complexity to the investigation of outfall discharges particularly leading to the alteration of the initial mixing behavior of dense outfalls, and accordingly is worthwhile to be studied. The situation in which the ambient flow is perpendicular to the dense jet discharge has been known as a buoyant jet in cross-flow (JICF). As a result of the interaction between the buoyant jet and the cross-flow, the deflection of jet along the ambient water and momentum and energy exchange between them occur [30]. Besides to this cross-flow influence, the interplay of discharge momentum and buoyancy forces acts as a governing impact on the jet trajectory [31]. Thus, a highly complex three-dimensional jet flow trajectory is expected for the outfall discharge. A definition sketch of dense jet flow behavior while issuing into cross-flow, including the key flow parameters of interest is demonstrated in Fig. 1.

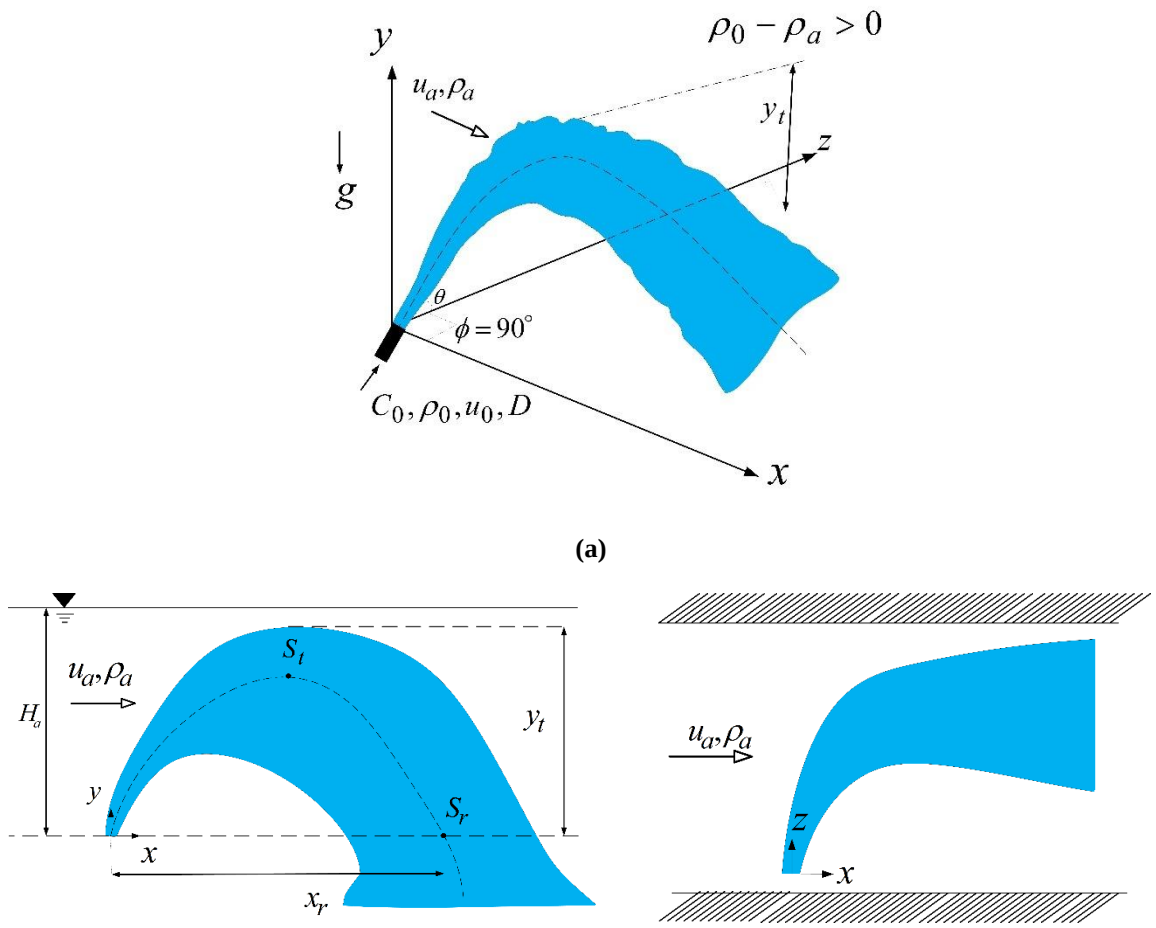

Fig.1 Schematic definition of inclined dense jet flow influenced by perpendicular cross-flow **(a)** 3D trajectory, **(b)** front view, and **(c)** top view

(where u, D, ρ, C, H, S, θ, and ϕ are the velocity, nozzle diameter, density, concentration, water depth, dilution, discharge angle, and angle of ambient cross-flow relative to the discharge propagation at the source, respectively, indexes *0* and *a* represent the discharge and ambient characterises, respectively, and indexes *t* and *r* denote the terminal and return point characterises, respectively.)

Among the few works focused on the dense discharge in flowing water, the following literature can be mentioned. Tong and Stolzenbach [32] investigated the dilution performance of 60° and vertical heated saline effluent jets using temperature as a tracer and a photogrammetry technique and presented a relatively insensitive dilution amount to the discharge source inclination for the condition tested. In another study, Roberts and Toms [33] extensively examined 60° inclined and vertical dense jets for different co-flow and counter-flow cases as well as only five tests for the perpendicular cross-flow with a 3D trajectory using photogrammetry and suction sampling techniques. They showed that there is a dependency of dilution and geometrical characteristics to a cross-flow based Froude number defined as $u_r F =$

$\frac{u_a}{u_0} \times \frac{u_0}{\sqrt{g_0' D}}$ (where F is the jet-densimetric Froude number and g_0' is the modified acceleration due to gravity) and the 60° discharge jets perform more preferable over the vertical ones in most cases. Lindberg [34] identified three different flow regimes based on the definition of $u_r F$ (namely negligible cross-flow, weak cross-flow, and strong cross-flow) and reported geometrical parameters of the jet flow using the experimental tests of inclined negatively buoyant jets in a water tow tank. Later, Gungor and Roberts [14] examined the concentration flow field of vertical dense jets with a 2D trajectory using a LIF technique over the cross-flow range of $0.21 < u_r F < 0.92$ in a quiescent tow tank. The increase in the dilution of terminal rise height and impact point were observed with the increase of current speed for the experimental condition tested. Vertical dense jets issuing into ambient currents also discussed in another study by Ben Meftah et al. [35–36] for $u_r F = 1.0$ and 1.1.

Furthermore, Lai and Lee [37] studied the concentration flow field using LIF for a 60° dense jet influenced by a perpendicular cross-flow with a 3D trajectory, and only terminal rise data including dilution and location was reported according to the field of view considered in their study. They argued that the jet trajectory is predominantly impacted by the ambient current for a limit about $u_r F \geq 0.8$, and the detrainment has a negligible impact on the jet behavior for $u_r F \geq 2.0$. More recently, the mixing behavior of a 45° dense jet discharging into co-flow and counter-flow currents in a quiescent water tow tank was investigated using the LIF approach by Jiang et al. [38]. Based on their results, the source discharge characteristics can mainly affect the flow behavior within $u_r F < 1.0$ (i.e., jet-dominated regime), however, the ambient currents can play key roles in the mixing behavior of dense jets outside this range (i.e., current-dominated regime).

The literature discussed above are mainly concerned with the dense jet discharges impacted by flow currents (co-flow and counter-flow) with a 2D trajectory in which the flowing waters were resembled by a towing system (it should be mentioned that this simulation may lead to some differences in the jet discharge behavior compared to when releasing in a real flowing environment). Also, the majority of collected data were within the jet-dominated regime or within the strong cross-flow regime where the jets become nearly horizontal and have minimum impact on the seabed because of moving quickly into the far-field region (i.e., outfall signature is considerably eliminated) [14]. However, as a representation of realistic site conditions that may occur, investigations on the mixing behavior of perpendicular cross-flow currents within the range $1.0 \sim < u_r F < \sim 1.6$, regular cross-flow dictated regime [31], should

be further intensified. In addition, the paucity of knowledge on the understanding of deploying different dense discharge angles issuing into dynamic waters still remains. A study of inclined configurations and relative perpendicular alignment of dense jet discharges with the current direction can provide a better picture of proper design as well as discharge performance of dense outfalls, particularly when utilizing them close to the shoreline regions.

This study presents the first attempt to experimentally simulate the dense discharges with different source inclinations while issuing into perpendicular cross-flow currents having 3D trajectories with the aid of the imaging approach of LIF. By applying the dimensional analysis, it is shown that the dense jet flow behavior is mainly dependent to cross-flow based Froude number and discharge angle. Accordingly, the main objectives behind this study are to reduce the negative impacts of dense discharges into marine environments by addressing the combined effects of discharge angles and flowing currents' strength in the discharge regions. The major flow features of inclined dense JICFs are comparatively studied and design instructions are provided. The analysis of the obtained results also covers the instantaneous and time-averaged flow visualizations, jet trajectory examination, geometrical and dilution characteristics of jet flow, jet widening, and variance of concentration. For protecting the receiving water bodies and improving the management of outfall discharges, such information is of significant importance.

The remainder of this paper is structured as follows. Section 2 includes the dimensional analysis for the inclined dense JICFs and the experimental procedure. Results and discussion are presented in Section 3. In detail, general observation of flow behaviors and jet trajectory are discussed in Sections 3.1, and 3.2, respectively. Section 3.3 presents the effect of $u_r F$ and discharge angles on the main flow parameters, and the relevant empirical equations. Jet widening and variance of concentration are explained in Sections 3.4, and 3.5, respectively. Finally, Section 4 concludes the paper with some concluding remarks.

2 Methodology and Experimental Conditions

2.1 Dimensional Analysis

There are two basic assumptions that should be considered for deploying the dimensional analysis for the case of a dense JICF. Viscosity impacts are not involved, and the discharges are completely turbulent. Besides, the Boussinesq approximation is valid [39]. For this case, the main flow parameters, including dilution (S_r and S_t) and geometrical (x_r and y_t)

characteristics, can be described as a function of ambient cross-flow properties and initial source conditions [33,36]:

$$x_r, y_t, S_r, S_t = f(Q_0, B_0, M_0, u_a, \phi, \theta) \quad (1)$$

where Q_0 is the discharge volume flux, $B_0 (= g_0^{'} Q_0)$ is the discharge buoyancy flux (where $g' = g(\rho - \rho_a)/\rho_a$), M_0 $(= u_0 Q_0)$ is the discharge momentum flux. With respect to the definitions for velocity and length scales, which are relevant to the fluxes of discharge volume, discharge buoyancy, and discharge momentum, the following relationships can be written [14,20,33]:

$$u_c = {B_0^{1/2}}\Big/{M_0^{1/4}} \quad (2)$$

$$l_M = {M_0^{3/4}}\Big/{B_0^{1/2}} \quad (3)$$

$$l_Q = {Q_0}\Big/{M_0^{1/2}} \quad (4)$$

where u_c is the velocity scale, l_M is the jet-to-plume length scales, and l_Q is the discharge length scale. Following the dimensional analysis and considering that the jet dilution properties can be expressed as $S = g_0'/g' = (\rho_0 - \rho_a)/(\rho - \rho_a)$ due to the validity of Boussinesq assumption [20], Eq. (1) can be rewritten as below for the geometric scales of flow trajectory and dilution properties [33]:

$$\frac{x_r}{l_M} or \frac{y_t}{l_M};\ S_r \frac{l_Q}{l_M} or\ S_t \frac{l_Q}{l_M} = f(\frac{l_M}{l_Q}, \frac{u_a}{U_c}, \phi, \theta) \quad (5)$$

The right-hand side of above relationship can be replaced by some equivalencies for a round turbulent buoyant jet with a source diameter of *D* which are presented as follows [20,33]:

$$l_M = (\frac{\pi}{4})^{1/4} DF;\ \frac{l_M}{l_Q} = (\frac{\pi}{4})^{-1/4} F;\ \frac{u_a}{U_c} = (\frac{\pi}{4})^{-1/4} u_r F \quad (6)$$

where u_r is the ratio of ambient cross-flow to jet velocity ($u_r = u_a/u_0$). Thus, Eq. (5) can be stated as [33]:

$$\frac{x_r}{DF} or \frac{y_t}{DF};\ \frac{S_r}{F} or \frac{S_t}{F} = f(F, u_r F, \phi, \theta) \quad (7)$$

where the parameter of $u_r F$ denotes to the definition of cross-flow based Froude number. This definition indicates the relative strength of ambient flow current to buoyancy [40]. According to the Eq. (7), this can be concluded that the jet dilution properties scale with *F*, and the geometric parameters scale with *DF*. In the case of $F (or \frac{l_M}{l_Q}) \geq 20$, the jet-densimetric Froude

number can be eliminated as an individual term in the list of dependent parameters or, in other words, the influence of the source volumetric flux is insignificant [13,27,37].

Based on these assumptions and for the case of having a perpendicular angle between cross-flow and the discharge propagation at the source ($\phi = 90°$), Eq. (7) can be considered as follows:

$$\frac{x_r}{DF} \text{ or } \frac{y_t}{DF}; \frac{S_r}{F} \text{ or } \frac{S_t}{F} = f(u_r F, \theta) \tag{8}$$

Hence, the values of $u_r F$ and discharge angle play key roles in determining the jet's dilution properties and trajectory for the case of dense JICF.

2.2 Experimental Setup and Procedures

In this study, the experimental investigations of submerged dense jet discharge into the dynamic ambient environment were conducted using the LIF setup, which can capture the flow structure evolutions as well as measure the jet trajectory and concentration distribution of the discharge system. These experimental tests were run at the Hydraulics Laboratory of the University of Cagliari, Sardinia, Italy. The flume used in these systematic experiments had 6 m length, 0.4 m width, and 0.5 m depth. A reservoir tank was also set in the proximity of the flume for water supply. This experimental flume was made of glass to be able to have an appropriate flow visualization. The flow rate in the flume was controlled using a ball valve close to the entrance tank. An adjustable weir placed at downstream was also used to control the head of flow. The experimental flume is shown in Fig. 2.

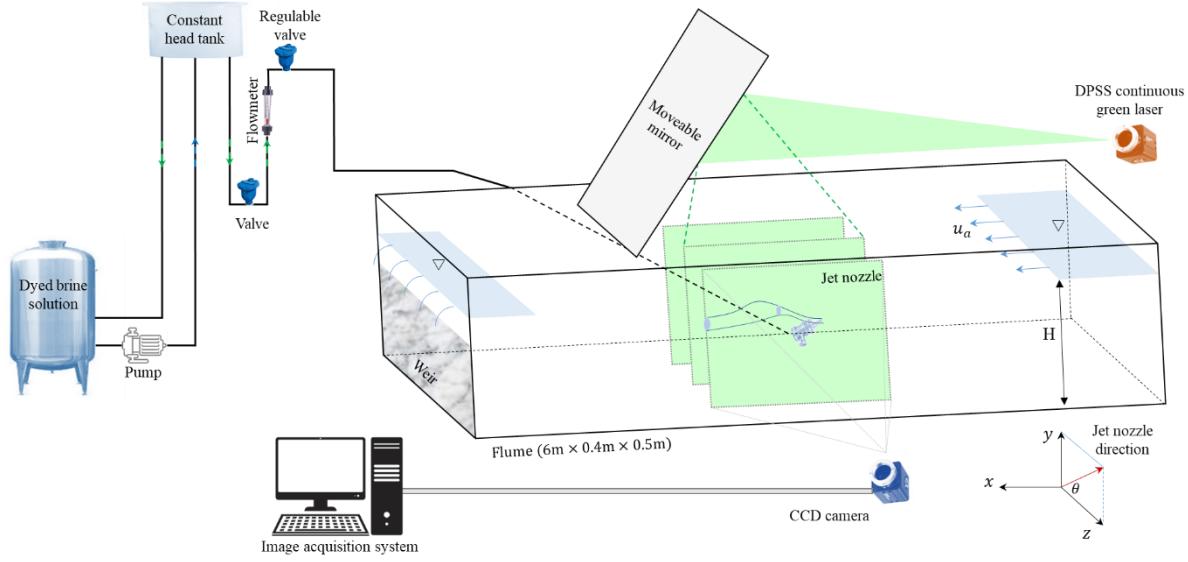

Fig. 2 Schematic depiction of the LIF experimental setup

The jet discharge was located at a distance of 3 m from the flume entrance to ensure the ambient flow was fully developed. The nozzle was a round pipe with an inner diameter of 3.2 mm, and the length of nozzle pipe before the outlet was long enough to make sure that the discharge flow regime was well-controlled. The discharged brine came from a constant-head closed hydraulic circuit: three separated zones were considered in the discharging reservoir, so that one of them was for reducing the chaotic of inflow to the reservoir, the second zone was connected to the discharge nozzle, and the third zone provided a constant water level in the previous zone for keeping a stable discharge rate in the flume. It should be mentioned that the discharge rate from the nozzle was also controlled using a flowmeter during each experiment run. In the present study, three nozzles with discharge angles of 30°, 45°, and 60° relative to the horizontal were applied, with a distance of nozzle tip to the flume bottom of 0.1 m.

Saline water was used as the effluent in the laboratory experiments, and fresh tap water was used as the ambient water. The density of the effluent was measured using a handheld bubble density meter. Temperatures of both source discharge and ambient water were kept to be about 25 ± 1 °C. A range of discharge densities from 1030 to 1065 kg/m^3 was also considered to obtain the desired density difference. Also, the brine jet was temporarily permitted to discharge into the flume before running the experiments to achieve a steady state flow condition. Due to the lower density of ambient water compared to the effluent discharge density, a negatively buoyant discharge (NBJ) was generated. Table 1 presents the experimental conditions.

Table 1 Experimental Conditions

Runs	**Discharge Angles (°)**	$\boldsymbol{\rho_0}$ **(kg/m^3)**	**F**	**Discharge Buoyancy Flux** $(\boldsymbol{B_0 = g_0' Q_0})$	**Jet-to-plume Length Scale** $(\boldsymbol{l_M(m) = M_0^{3/4} / B_0^{1/2}})$	**Plume-to-cross-flow (Buoyancy) Length Scale** $(\boldsymbol{l_b(m) = B_0 / U_a^3})$	$\boldsymbol{u_r F}$	$\boldsymbol{g_0'}$ **(m/s^2)**
R1	30	1030	33.7	2.4693E-06	0.1014	0.0199	1.62	0.2963
R2	45	1030	33.7	2.4693E-06	0.1014	0.0199	1.62	0.2963
R3	60	1030	33.7	2.4693E-06	0.1014	0.0199	1.62	0.2963
R4	30	1035	31.2	2.8782E-06	0.0939	0.0232	1.50	0.3454
R5	45	1035	31.2	2.8782E-06	0.0939	0.0232	1.50	0.3454
R6	60	1035	31.2	2.8782E-06	0.0939	0.0232	1.50	0.3454
R7	30	1040	29.2	3.287E-06	0.0879	0.0265	1.40	0.3944
R8	45	1040	29.2	3.287E-06	0.0879	0.0265	1.40	0.3944
R9	60	1040	29.2	3.287E-06	0.0879	0.0265	1.40	0.3944

R10	30	1045	27.5	3.6958E-06	0.0829	0.0298	1.32	0.4435
R11	45	1045	27.5	3.6958E-06	0.0829	0.0298	1.32	0.4435
R12	60	1045	27.5	3.6958E-06	0.0829	0.0298	1.32	0.4435
R13	30	1050	26.1	4.1047E-06	0.0787	0.0331	1.26	0.4926
R14	45	1050	26.1	4.1047E-06	0.0787	0.0331	1.26	0.4926
R15	60	1050	26.1	4.1047E-06	0.0787	0.0331	1.26	0.4926
R16	30	1055	24.9	4.5135E-06	0.075	0.0364	1.20	0.5416
R17	45	1055	24.9	4.5135E-06	0.075	0.0364	1.20	0.5416
R18	60	1055	24.9	4.5135E-06	0.075	0.0364	1.20	0.5416
R19	30	1060	23.8	4.9223E-06	0.0718	0.0397	1.15	0.5907
R20	45	1060	23.8	4.9223E-06	0.0718	0.0397	1.15	0.5907
R21	60	1060	23.8	4.9223E-06	0.0718	0.0397	1.15	0.5907
R22	30	1065	22.9	5.3312E-06	0.069	0.043	1.10	0.6397
R23	45	1065	22.9	5.3312E-06	0.069	0.043	1.10	0.6397
R24	60	1065	22.9	5.3312E-06	0.069	0.043	1.10	0.6397

T_{ave} = 25 ± 1 °C, $Re_0 = 2100$, Discharge volume flux (Q_0) = 8.33E-06 (m^3/s), Discharge momentum flux ($M_0 = U_0 Q_0$) = 8.64E-06 (m^4/s^2), Jet-to-cross-flow length scale ($l_m = {M_0^{1/2}}/{U_a}$) = 0.0589 (m), Discharge length scale ($l_Q = {Q_0}/{M_0^{1/2}}$) = 0.0028 (m), H_a = 0.271 m

In our experimental tests, a small amount of fluorescent Titanium dioxide dye as a tracer, which tends to emit on the same wavelength of the incident light, was added to the source flow containing saline water. After discharging the effluent, the diode-pumped solid-state (DPSS) continuous green laser with an output power of 5 W and wavelength of 532 nm caused the dye to fluoresce and emit light. The emitted lights were captured by the high-speed charge-coupled device (CCD) camera, Mikrotron EoSens 4CXP CoaXPress, at 50 frames per second (to ensure that the flow fields on two consecutive frames were uncorrelated) with a maximum resolution of 2336 × 1728 pixels. The acquisition mode was continuous, and the exposure time was 4000 second. The captured images were set to be stored in Mono8 bit resolution, i.e., 256 grayscale levels, to reduce the space taken up by them. Thus, the recorded images displayed a jet flow with a bright color in a dark background where the light intensity level of each pixel could be shown in different 256 values that range from pure black to pure white, corresponding, as the amount of fluorescent dye was small enough to ensure a linear proportionality between the salt concentration and the emitted light intensity, to the salt concentration.

An F-mount 50 mm lens with f/1.4 was used to get better sensitivity of the captured images and to improve the area of coverage. Moreover, an orange filter was installed on the camera to

cut off light below 550 nm and filter out the scattered lights from the green laser. As a result, the quality and contrast of obtained images were enhanced. The camera was connected to a computer using the PCI frame grabber with the four attached CameraLink cables. It should be mentioned that the laser reflections from the bottom and side walls of flume were prevented during the experimental tests by using black non-reflective materials.

Before discharges relevant to each run, a series of about 100 images of only background without the presence of NBJs was recorded and time-averaged to have a source for eliminating the unwanted lights not corresponding to the jet fluid concentration. In the next step, considering the camera capturing features, a series of more than 3,000 images from the flow development of each NBJ run was recorded. The background image was subsequently subtracted from the resulting image with the jet for the mentioned purpose of removing the excess lights.

In order to obtain the jet trajectory characteristics and concentration distribution contours, captured images needed further post-processing using a written MATLAB code, developed for the specific purposes of the present experiments. This code computes the light intensities of each pixel of the grayscale images and then turns them into color-coded versions. A statistical analysis, including the time-averaged frames of flow dynamic and their variance, was also obtained through the program by considering together the instantaneous frames. Subsequently, the concentration distribution fields and contours based on the non-dimensionalized C/C_0 parameter (where C_0 is the discharge concentration), were generated, showing the amount of mean concentration reduction (dilution level) compared to the initial concentration. Moreover, the axes were normalized by the nozzle diameter D, considering the origin of plots on the nozzle outlet.

This procedure was repeated by changing the position of vertical laser sheet emission through the width of the flume so that 8 different slices spaced about 25 mm apart were achieved. Apart from this experimental setup configuration, the horizontal emission of laser sheet at the level of nozzle port and vertical position of the camera at the top of the flume was also applied. By placing the obtained frames together using the Paraview visualization software tools, the 2D and 3D depictions of flow field were eventually formed. Fig. 3 illustrates the algorithm considered for post-processing the LIF images.

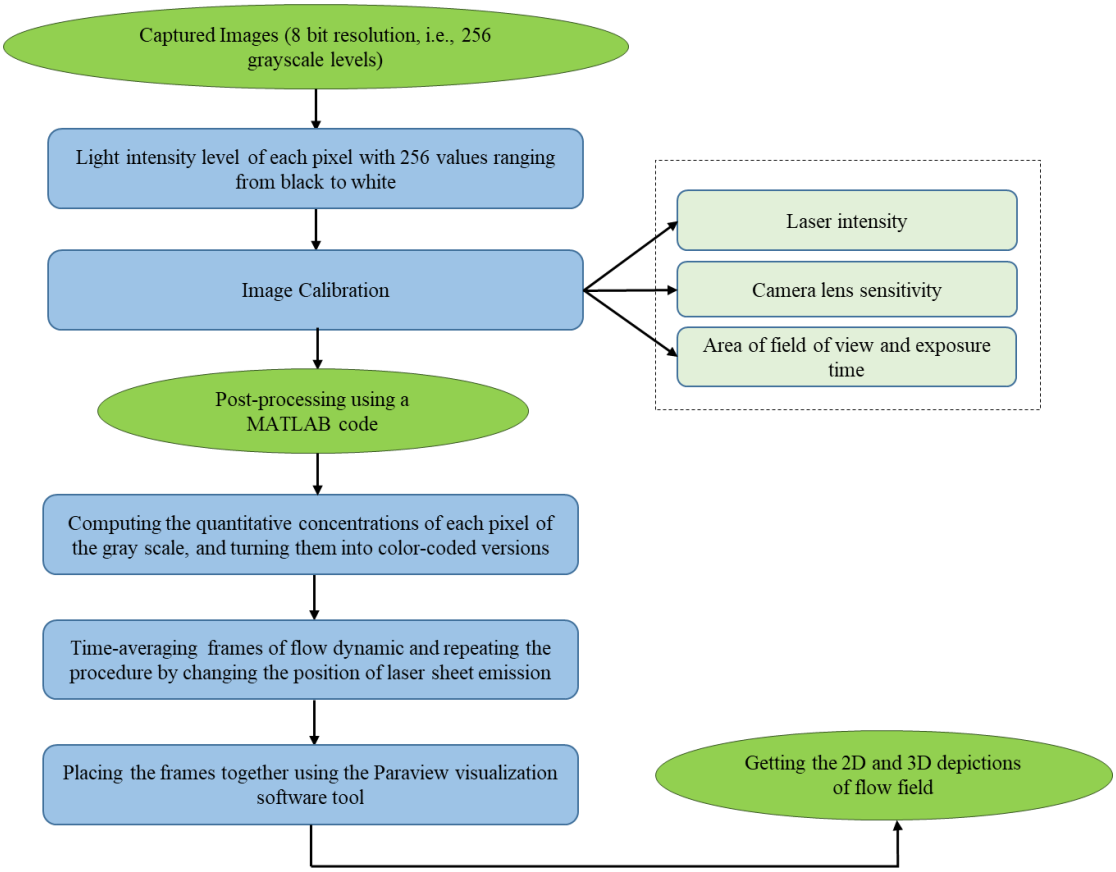

Fig. 3 Workflow for post-processing the LIF images

3 Results and Discussion

3.1. General Observation

3.1.1. Instantaneous Visualization

Some captured frames from the planes at different distances from the nozzle discharge point are illustrated in Fig. 4 which shows the instantaneous flow development for the experimental cases of R19 and R21. The low concentrations of jet discharges are indicated by dark gray, while the high concentrations are pointed out by pale gray. The jet brightness in the closeness of the outlet is high and as moving farther from the outlet the luminosity starts reducing, showing an increase in dilution due to the external fluid entrainment into the jet flow [29]. The general flow behavior of an inclined jet includes a first ascending phase in which the jet momentum force prevails the negative buoyant force and a subsequent descending phase under the impacts of the dominant negative buoyant force [15,36].

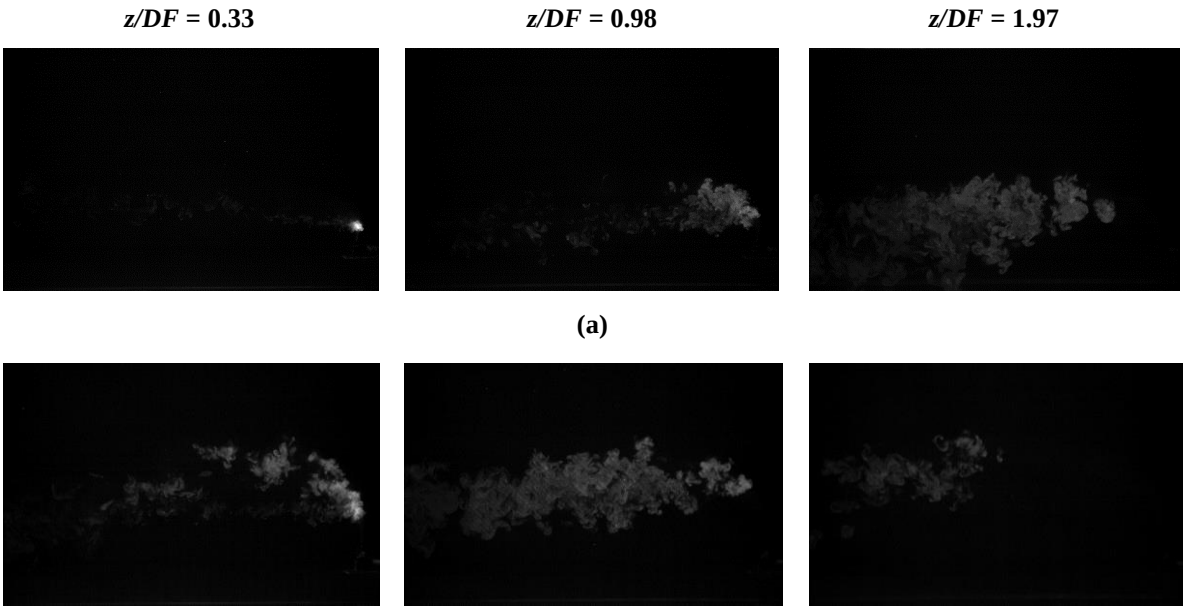

Fig. 4 Instantaneous flow visualization at different sections along the direction of flume width for the experimental cases of **(a)** R19 and **(b)** R21

In Fig. 5, the 3D instantaneous concentration fields are shown for the discharge angles of 30°, 45°, and 60° and experimental case numbers R7-9 and R19-21. These images were formed by placing frames together at a similar time from different sections within the recording period. The mixing mechanisms that play role in the jet dilution can be clearly demonstrated using the instantaneous flow observation. First, a primary flow with a well-defined structure is apparent in the ascending phase of the jet because of the initial momentum. However, beyond the reversal point of jet movement, groups of tracer fluid can gradually break apart from the main jet flow and indications of fluctuating flow motion, which is more chaotic as the jet propagates downwards, are visible, representing the dominance of negative buoyancy flow [15,41]. Two flow features occur on the upper and lower edges following the jet descending arm. The one corresponding to the upper edge is the rotating bundles of tracer facilitating the entrainment of ambient flow into the main jet flow. This indicates the prevailing effect of eddy motions in this border. Besides, the one relevant to the lower edge is the detrainment and falling away of fluid mass from the inner side of primary jet flow as a result of buoyancy instabilities, i.e., the unstable density gradient [15,37].

Regarding the impact of deploying different discharge inclination upon the flow behavior, discrepancy can be also reported despite similar general behavior. Buoyant instabilities are less prominent for shallower discharge angles owing to the higher z-direction momentum component, resulting in longer preserving the form of initial jet primary flow. Furthermore,

comparing the flow fields for the series of experiment with higher $u_r F$ (R7-9) with the ones with lower $u_r F$ (R19-21) can reveal less confinement and more spread of jet flow within the ambient environment when applying higher cross-flow based Froude numbers. This observation will be also discussed later in Section 3.4.

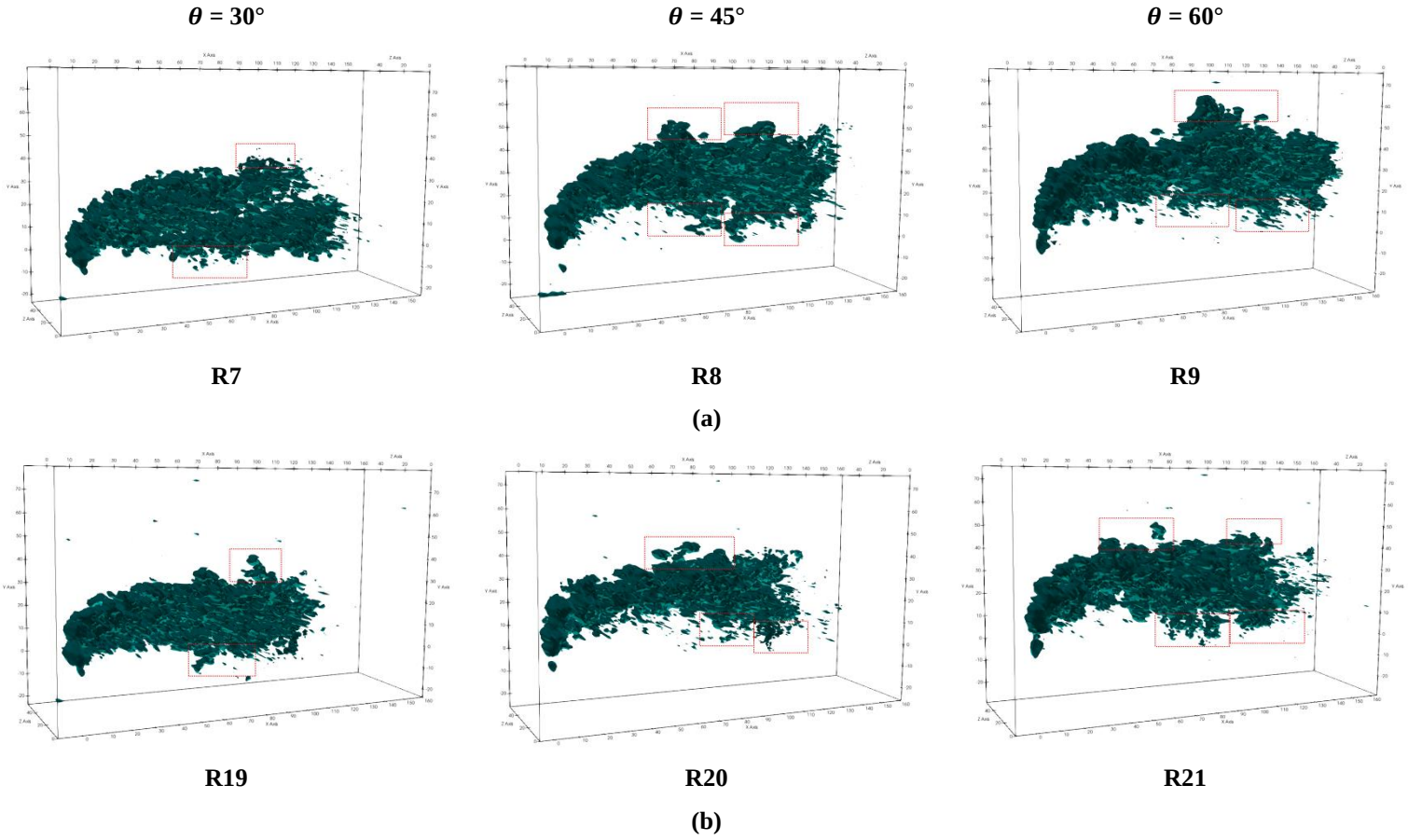

Fig. 5 Instantaneous concentration flow fields for the experimental case numbers of **(a)** R7-9 and **(b)** R19-21

3.1.2. Timed-averaged 3D Visualization

Considering the flow depiction through the sections and putting them together, the timed-averaged 3D of flow jet discharge behavior was obtained using Paraview software tool, as shown in Fig. 6. Generally, due to the initial velocity of inclined discharge flow, the rising trajectory occurs as the momentum force is dominant. The jet flow path also starts bending along the longitudinal direction of flume as a result of cross-flow current. The momentum force then reduces continuously and becomes equal to buoyant force where the maximum height of jet takes place. Afterward, the buoyant force overcomes the momentum of jet discharge and the falling stage of trajectory occurs [20,29,35]. Comparison of the discharge angles impact on the flow movement can be also highlighted with the following statements:

- for the case of 30°, movement of brine flow along the flume width was more progressive than the other discharge angles. This is mainly because of the higher z-direction momentum component of this angle.
- The terminal rise point of 60° discharge angle was higher than the other two angles.
- For the case of 60°, the longest jet trajectory was obtained, giving more time to the jet for having the interaction with the ambient flow.

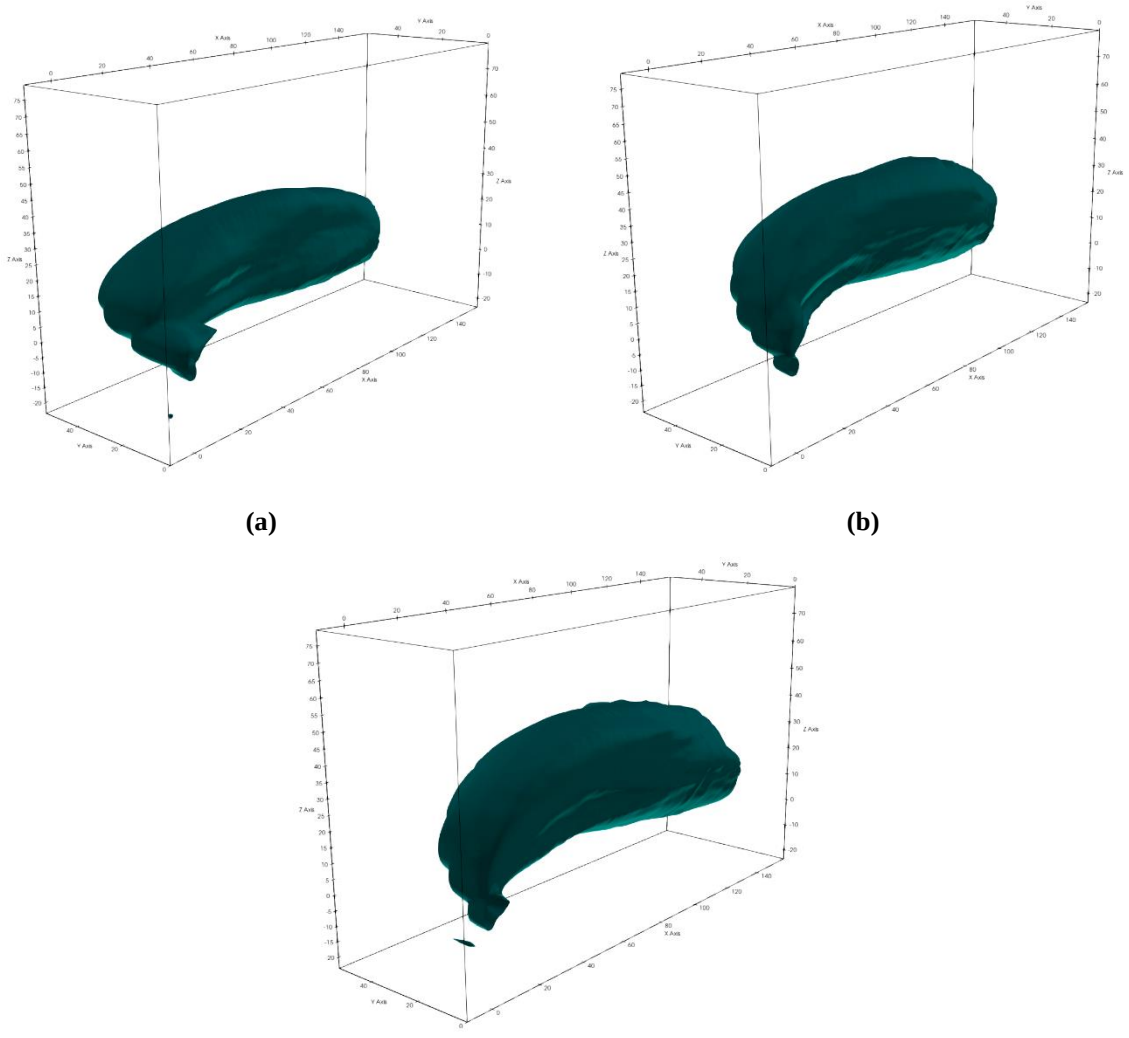

(a) **(b)**

(c)

Fig. 6 Timed-averaged 3D visualization of the jet discharge flow field for the experimental cases of **(a)** R19: θ = 30°, **(b)** R20: θ = 45°, and **(c)** R21: θ = 60° (iso-surface C/C_0 = 0.03)

Fig. 7 also illustrates the time-averaged 2D concentration profiles at three different cross-sections for the experimental cases of R19 and R21 with the discharge angles of 30° and 60°, respectively. Comparison of the concentration fields of 30° and 60° at a similar distance from the discharge point shows that applying the steeper inclination leads to the higher dilution levels. Dispersions of jet flow in the ambient water for the discharge angle of 60° are also

higher than that for the 30° angle, which can be an evident for the better dilution performance of the jet with 60° angle in the dynamic environment. Besides, the development of concentration flow field along the flume width reveals that the jet flow for the discharge angle of 30° first attempts to form an almost C-shape of concentration distribution with distinguishable upper and lower sides and it gradually generates more uniform distribution as moving farther from the discharge point at *z/DF* = 1.97. However, for the 60° angle, the jet flow forms a concentration distribution with only noticeable upper side in the closeness of discharge source at *z/DF* = 0.33 and then the uniform distribution starts appearing immediately from *z/DF* = 0.98.

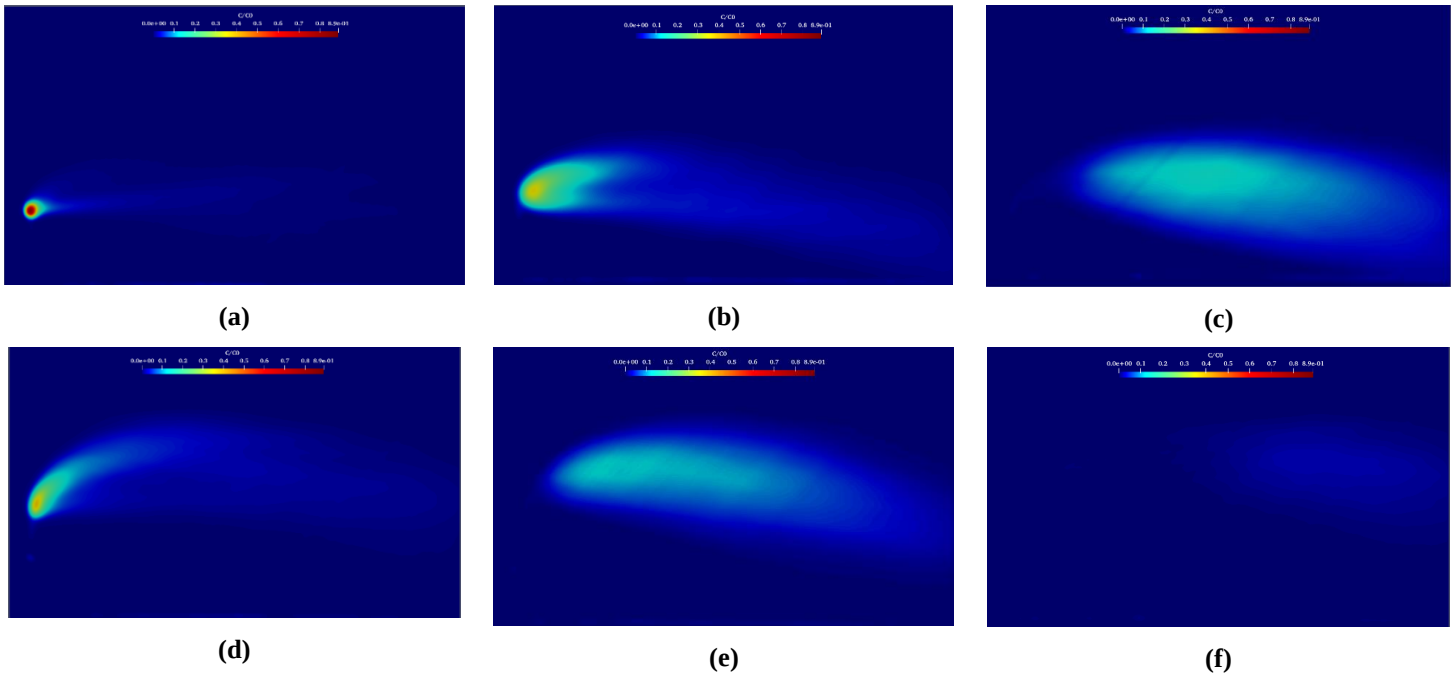

Fig. 7 Timed-averaged 2D visualization of concentration flow field for the experimental case of **(a-c)** R19 at the cross-sections of *z/DF* = 0.33, 0.98, and 1.97, respectively, and for the experimental case of **(d-f)** R21 at the at the cross-sections *z/DF* = 0.33, 0.98, and 1.97, respectively.

3.2. Jet Trajectory

The jet trajectory as a track of flow discharge path can be defined based on the locus of maximum concentration, as shown in Fig. 8 in two different front and top views. According to the obtained results, the following conclusions can be drawn.

- Jet flow penetration along the width of flume increases with the reduction of discharge angle from 60° to 30°, due to the higher momentum in the z direction for the shallower angles.

- 60° discharge angle leads to the observation of jet flow in higher height from the nozzle tip, compared to the other two angles.
- From both top and front views, longest trajectory can be seen for the discharge angle of 60°.
- The jet of 60° bends more sharply in the direction of ambient current compared to the other two angles.
- Rapid ascending and gradual descending phases can be observed for all the jet flows.

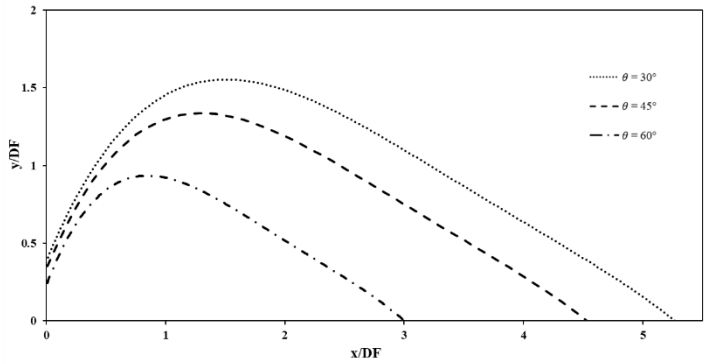

(a)

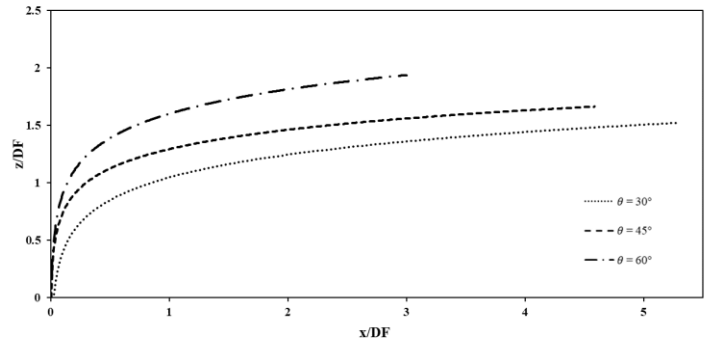

(b)

Fig. 8 Jet centerline trajectories based on the **(a)** front view and **(b)** top view for the experimental cases of R7-9

3.3. Effects of $u_r F$ and Discharge Angle

3.3.1. Geometrical Characteristics

One of the important factors in the study of brine jet discharges that should be considered is the jet terminal rise height. Getting the information of this parameter gains significance when dealing with the discharges in shallow currents. Maximum jet terminal rise height for our experimental tests were obtained based on the 10% of the transverse maximum concentration at the location of jet maximum height [16]. In Fig. 9, the changes in $\frac{y_t}{DF}$ parameter versus $u_r F$

for the three tested inclined angles are presented. The related data of few available studies for the jet of 60° with a 3D trajectory in the range of u_rF covered herein is also shown for comparison [32,33,37]. In the region of u_rF studied in our experimental tests which is out of jet-dominated zone, the maximum terminal rise height tends to decrease by rising the u_rF for all the inclined angles. Larger values of cross-flow based Froude numbers deflect the initial jet direction toward the direction of ambient current at closer distances to the nozzles. This result is in accordance with the one obtained in the related studies [32,33,37] and the ones for vertical dense jets in a cross-flow [14,36]. However, the decrease in the terminal rise point with the increase of u_rF has not been reported considerably in the studies conducted in the range of $u_rF < \sim 1.0$ [32,33,37]. It can be an evident for the different jet discharge behavior while issuing in the regimes of jet- and current- dominated. Therefore, the inclusion of data in the jet-dominated regime for the prediction of inclined jet discharge behavior in cross-flow currents in the range $1.0\sim < u_rF < \sim 1.6$ cannot be valid. This also intensifies the importance of study in this critical range.

From the comparison of discharge angles impact on the obtained terminal rise parameter, this can be expressed that this parameter is about 10% and 36% higher than for the jet of 60° compared to the 45° and 30°, respectively, in the range of u_rF tested. The semi-empirical power-law dependency of maximum jet terminal rise height to cross-flow based Froude numbers for the 30°, 45°, and 60° discharge angles was also extracted. According to Table 2, it can be stated that the jet terminal rise changes with the u_rF to the power of $\sim(u_rF)^{-0.5}$ for the jet of 60° while this dependency is about $\sim(u_rF)^{-0.65}$ for both the jets of 30° and 45°.

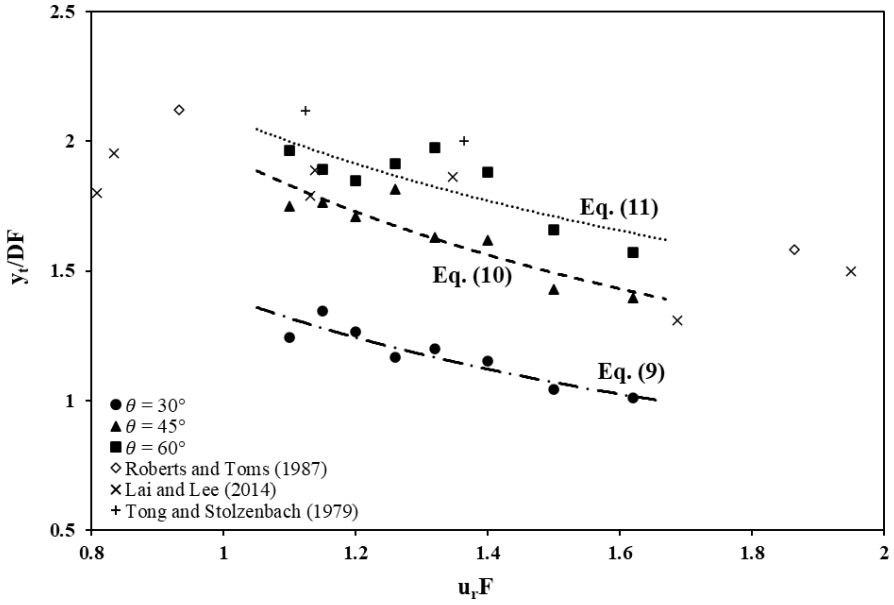

Fig. 9 Terminal rise height for the discharge angle of 30°, 45°, and 60°

Another important geometrical characteristic in the study of brine jet discharges is the horizontal location of the jet impact point or return point. It is worthwhile mentioning that attention should be given to the small difference between these two definitions although both want to say how long is the trajectory of flow path and to show the near-field region influenced by the initial mixing. This parameter indicates the horizontal distance from the discharge point to the location where the jet returns to the level of nozzle tip and addresses the point that the jet discharge has exposure with the benthic organisms which may be environmentally important [39].

The $\frac{x_r}{DF}$ variations based on the $u_r F$ are demonstrated in Fig. 10. It should be mentioned that there is a lack of available horizontal location data for the $u_r F$ range of almost above 1 in the literature. Thus, the results of this work can elucidate how this parameter can change within the critical range of $u_r F$ between 1 and 2, i.e., out of the jet-dominated zone. With the increase of $u_r F$, there is a small alteration in the $\frac{x_i}{DF}$ parameter for our cases studied. However, with the rise of $u_r F$ up to 1, the $\frac{x_i}{DF}$ parameter increased for the vertical dense jets according to the literature [14]. This result reveals that the difference in the jet-dominated and ambient cross-flow dominated zones should not be ignored regarding their effects on the jet return point. Additionally, the jet return points resulted from the discharge angle of 60° are higher than the two other angles. So that its corresponding results are about 16% and 41% higher than that of 45° and 30°, respectively. The semi-empirical power-law dependency of the jet return point to cross-flow based Froude numbers for the 30°, 45°, and 60° discharge angles is also presented in Table 2.

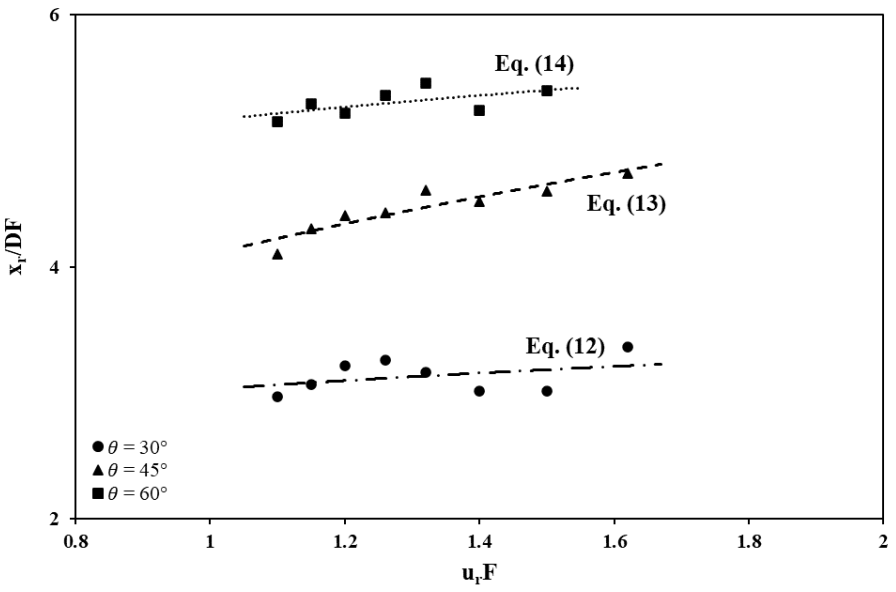

Fig. 10 Horizontal return point location for the discharge angle of 30°, 45°, and 60° (data for the $u_rF = 1.62$ is not identified)

Table 2 Semiempirical equations corresponding to the geometrical characteristics

θ (°)	$y_t/DF = a\,(u_rF)^b$		Eq.	$x_r/DF = c\,(u_rF)^d$		Eq.
	a	b		c	d	
30	1.4	- 0.67	(9)	3.03	0.12	(12)
45	1.95	- 0.65	(10)	4.1	0.31	(13)
60	2.1	- 0.5	(11)	5.16	0.11	(14)

3.3.2. Dilution Characteristics

For the purpose of environmental impact assessment, the level of dilution at some specific points along the jet trajectory such as the centerline peak point is of the utmost importance in the study of brine outfalls. In Fig. 11, the variations of $\frac{S_t}{F}$ parameter versus the u_rF values for the different discharge angles of 30°, 45°, and 60° are shown, and the relevant semi-empirical equations are determined accordingly (see Table 3). The available data from previous studies for the jet of 60° with a 3D trajectory in the range of u_rF covered herein is also presented for comparison. It reveals that the obtained results are in a close agreement with the previous measurements [32,33,37].

Accordingly, the amounts of dilution at the jet terminal rise height are enhanced with the increase of u_rF in the tested range, showing the direct proportionality of cross-flow based Froude number to the mixing level. Regarding the influence of discharge angle, the jet with an

angle of 60° leads to higher dilutions. This increase in dilution at the terminal point is about 39% and 55% compared to the 45° and 30° angles, respectively. In addition, the associated semi-empirical equations indicate more sensitivity of $\frac{S_t}{F}$ parameter to the increase in the $u_r F$ values for the discharge angles of 60°. Hence, these results confirm the better mixing performance of dense inclined jets with 60° over the two other angles.

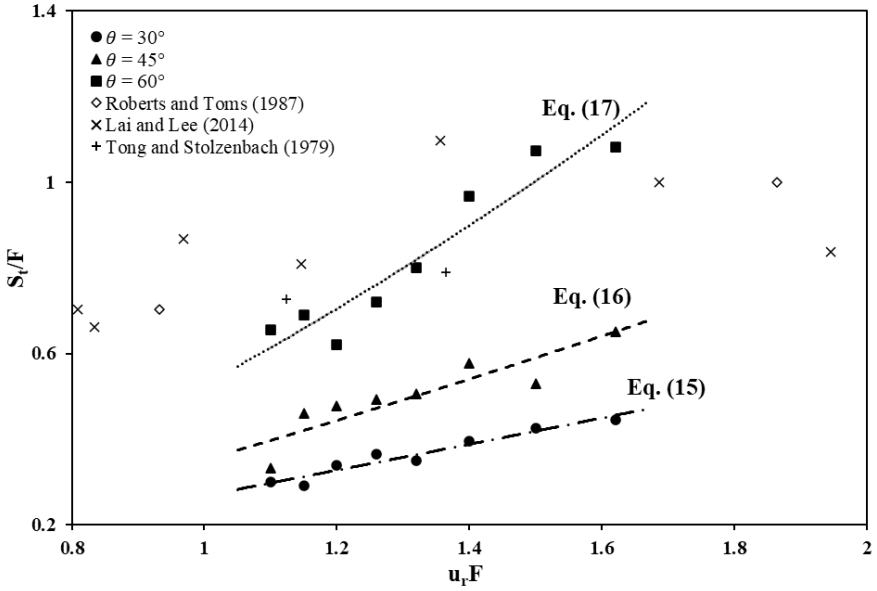

Fig. 11 Dilution at the terminal point for the discharge angles of 30°, 45°, and 60°

The minimum dilution at the return point of jet trajectory to the level of nozzle discharge is considered as the dilution at the jet return point. From the point view of optimal outfall design, maximum dilution should be achieved in the near-field region. This parameter is also a key for benthic impact management as a representation of the maximum substrate concentration [31]. Consequently, study of dilution amount at the jet return point is of particular interest to the design, operation, and regulation of this outfall applications. In Fig. 12, the changes in $\frac{S_r}{F}$ parameter according to $u_r F$ for our test cases are compared. The semi-empirical power-law dependency of minimum dilution at the jet return point to cross-flow based Froude numbers is also obtained and presented in Table 3. Dilution at the jet return point has an increasing trend with increasing cross-flow magnitude. $\frac{S_r}{F}$ results are almost 20% higher for the inclined angle of 60° in comparison with the ones for the case of 45°. Besides, the return point dilution for the 60° jet is more than twice of that for the 30° jet. The obtained dilution results can be ascribed to the longest flow path trajectory for the 60° jet, as it provides higher surface available for

entrainment of the external fluids and therefore more dilutions. These outputs highlight the importance of leveraging from the source discharge inclination and the cross-flow based Froud number to enhance dilution.

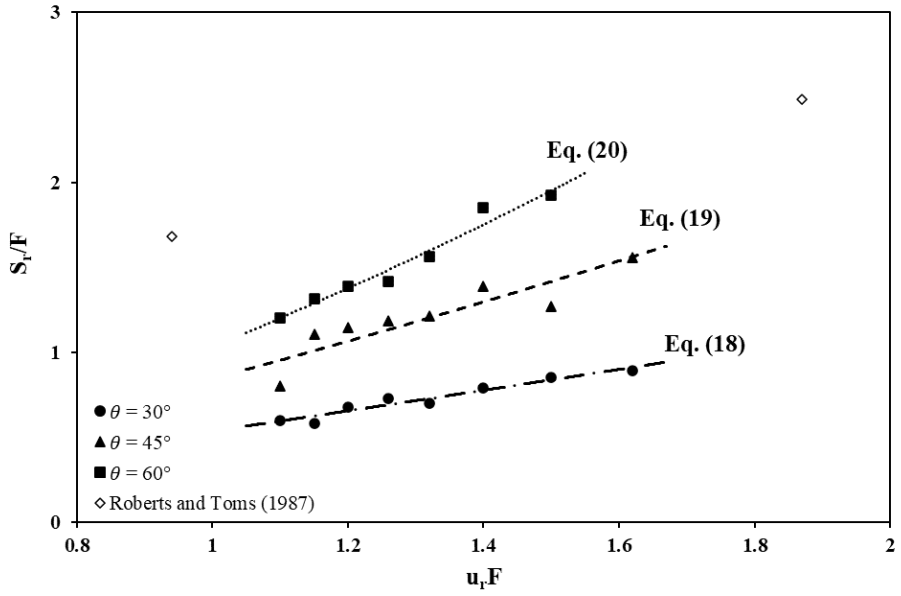

Fig. 12 Dilution at the jet return point for the discharge angle of 30°, 45°, and 60°

Table 3 Semiempirical equations corresponding to the dilution characteristics

θ (°)	$S_t/F = a\,(u_rF)^b$		Eq.	$S_r/F = c\,(u_rF)^d$		Eq.
	a	**b**		**c**	**d**	
30	0.26	1.1	(15)	0.53	1.1	(18)
45	0.35	1.28	(16)	0.84	1.27	(19)
60	0.54	1.58	(17)	1.03	1.56	(20)

3.4. Jet Widening

Study of the jet widening along the trajectory can also highlight the behavior of jet flow development and the role of discharge angle in the mixing and dilution performance of dense jets. In Fig. 13, normalized concentration profiles at different downstream cross-sections for the three discharge angles are presented. b_c represents the distance between the jet centerline and the location where the concentration is $e^{-1}C_{Max}$ on a cross-section, where C_{Max} is the local centerline tracer concentration. Based on Fig. 13 (a), in close proximity to the jet release point, the concentration profile is a little wider for the 30° than the other tested discharge angles, which can be attributed to the higher initial momentum component of the jet in the z-direction (along the flume width) with a shallower angle. However, this component vanishes for all cases

farther from the nozzle. The 60° jet has taken a further path up to a section far from the nozzle compared to the other jets. It provides a longer time for interacting with the external fluid and entraining ambient flow. Accordingly, the corresponding widening would be higher for the jet of 60°.

As shown in Fig. 13 (b) (which can be a demonstration of how the inner and outer edges of jets are behaving along the trajectory), the inner half for the discharge angle of 60° spreads wider than the outer half while for the angles of 30° and 45° the outer half is wider compared to their inner half. It has roots in the higher momentum values, in the z direction, for the two shallower inclinations. Moreover, the comparison of jet widening for the discharge angle of 60° with two different cross-flow based Froude numbers (Fig. 13 (c)) reveals that applying lower $u_r F$ values leads to a more confined jet, showing the limited available surface for interacting with ambient flows and lower level of dilution accordingly [42]. Hence, study of the jet widening results confirms the data from the analysis of discharge angle and $u_r F$ impacts on the dilution rate.

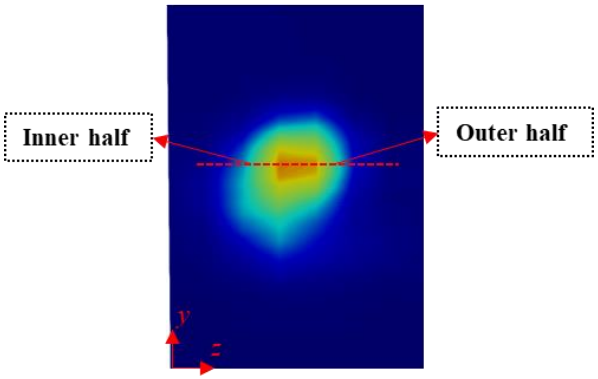

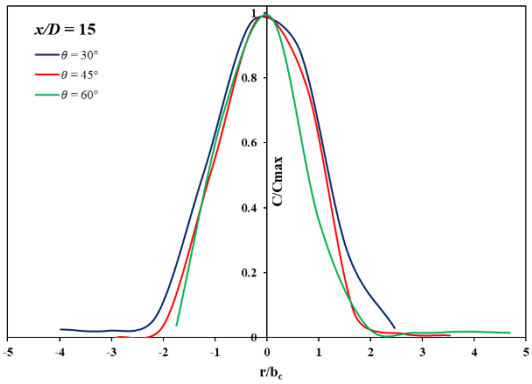

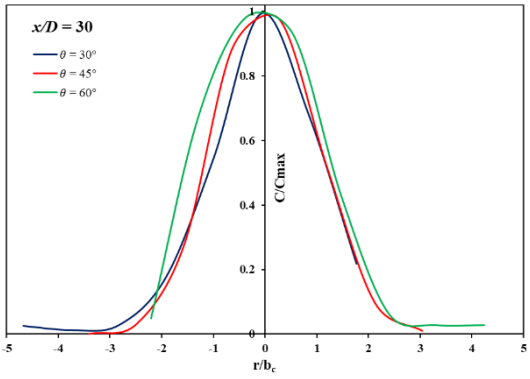

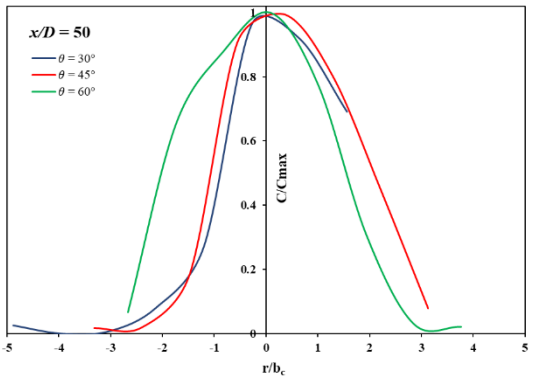
x/D = 50
θ = 30°
θ = 45°
θ = 60°
C/Cmax
r/b_c

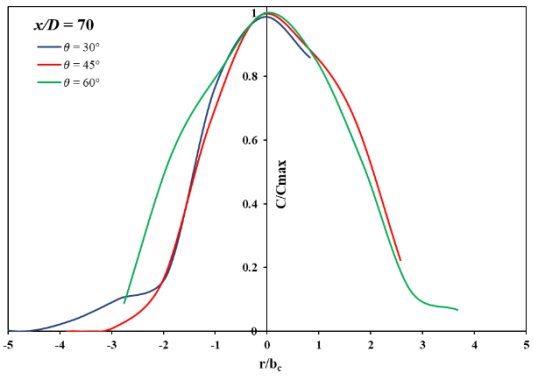
x/D = 70
θ = 30°
θ = 45°
θ = 60°
C/Cmax
r/b_c

(a)

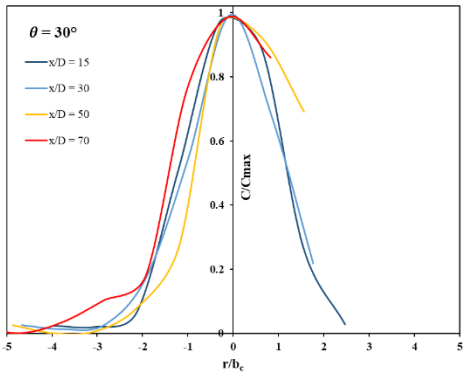
θ = 30°
x/D = 15
x/D = 30
x/D = 50
x/D = 70
C/Cmax
r/b_c

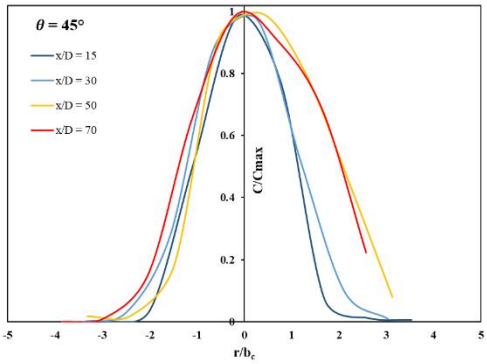
θ = 45°
x/D = 15
x/D = 30
x/D = 50
x/D = 70
C/Cmax
r/b_c

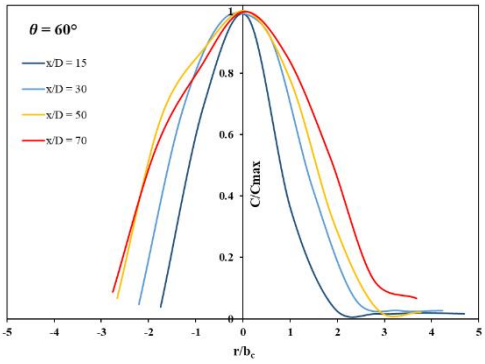
θ = 60°
x/D = 15
x/D = 30
x/D = 50
x/D = 70
C/Cmax
r/b_c

(b)

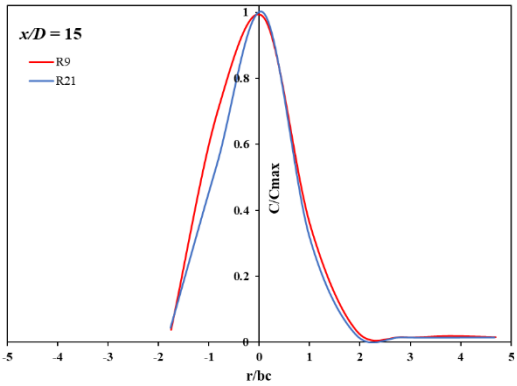
x/D = 15
R9
R21
C/Cmax
r/bc

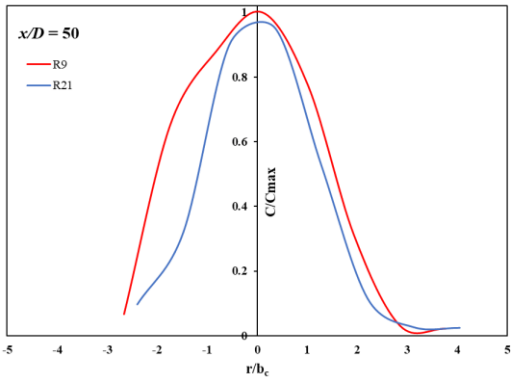
x/D = 50
R9
R21
C/Cmax
r/b_c

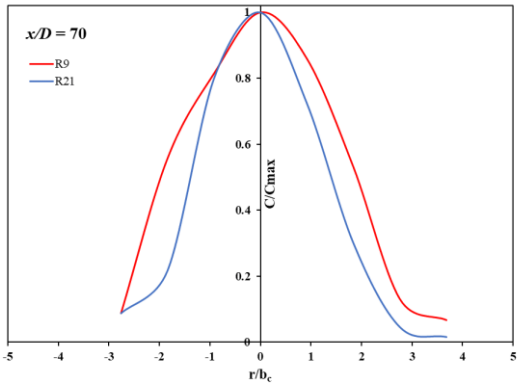

(c)

Fig. 13 Jet widening profile over the lines covering the jet flow width for **(a)** different angles and constant cross-section, **(b)** different cross-sections and constant angle for the experimental cases of R7-9, and **(c)** comparison of R9 and R21 at three different cross-sections

3.5. Variance of Concentration

Profiles of variance of concentration ($C^2/Cmax^2$), non-dimensionalized by the square of the maximum concentration, for the experimental cases of R7-9 and R19-21 are shown in Fig. 14. The concentration variance is proportional to stirring and is one of the turbulent mixing features. According to the obtained results, a bimodal distribution can be observed in the variance profile with a minimum level in the centerline region of jet. During the flow development, the core of the jet is very little influenced by the ambient water and the minimal variance in this region is the evident of this fact. In addition, increases toward the lower and upper sides can be seen in the variance profiles. This increase for the upper boundary is higher, which can be ascribed to the onset and development of Kelvin-Helmholtz (KH) instability structures and subsequently breaking due to the buoyancy which is against their growth [42,43]. It results in abrupt light intensity fluctuations and high variance levels. As moving along the flume width, the bimodal distribution becomes also smoother and finally collapses into one line. This decrease in variance level has its roots in the reduction of momentum discharge with the increase of distance from the discharge point along the flume width and accordingly diminishing the interaction of the jet flow and ambient environments. Moreover, the comparison of Figs. 14 (a) and (b) shows that the variance level is higher when the jet is influenced by the ambient current with higher $u_r F$, revealing more variation of concentration and thus more signs of jet and ambient water interactions.

Regarding the variance changes for the tested discharge angles, the variance levels decrease from 30° to 60°. It shows higher jet oscillation or bimodal distribution, which is the reason for reducing the jet momentum, shortening the jet trajectory, and thereby decreasing the surface

available for dilution with external fluid. Since stirring enhances dilution only if stirring happens with the interaction of brine and freshwater, not of brine with other brine.

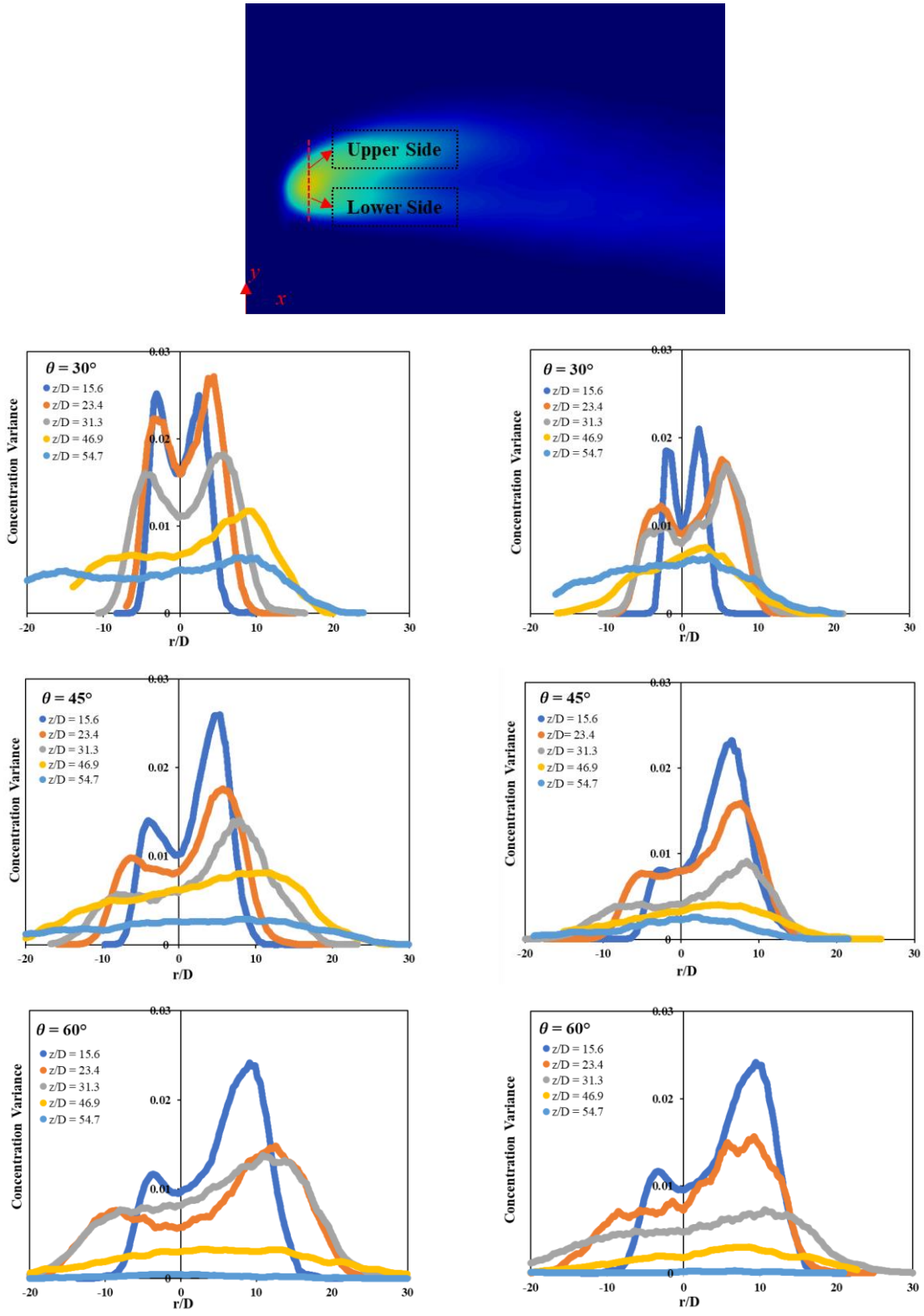

Fig. 14 Variance profiles along the flume width for the experimental cases of **(a)** R7-9 and **(b)** R19-21

4 Conclusions

For the efficient design of desalination outfalls, understanding the role of factors affecting the flow discharge and mixing behaviors is critical. The ambient hydrodynamics and discharge characteristics are among the important factors for the environmental risk assessment of an outfall. This study addressed the combined impacts of different flowing current's strength and discharge inclinations on the dense outfall performance. For this purpose, the mixing processes and concentration distribution of inclined dense discharges (including 30°, 45°, and 60°) issuing into the perpendicular current was investigated using the LIF experimental technique. The $u_r F$ parameter was selected in a way to stand in a critical range between about 1 and 2 in which the jets are considerably bent over.

Using the LIF experimentation, the instantaneous and time-averaged flow visualizations were obtained. Also, the major flow parameters (such as the terminal rise height, downstream position of the jet return point, and dilution at the terminal and jet return points) were quantified. The corresponding empirical equations were extracted, that can have further implications for the design of SWRO outfalls. The results revealed that almost all major flow parameters increased by the increase of cross-flow based Froude number within the range tested. In addition, with the increase of discharge angle from 30° to 45° and then to 60°, the geometrical parameters including downstream position of the return point and terminal rise height and the associated dilution levels were increased. The $\frac{x_r}{DF}$ for the jet of 60° was about 40% and 16% higher than that for the 30° and 45° jets, respectively. The $\frac{y_t}{DF}$ also increased by 36% and 10% when applying the 60° inclination in comparison with the 30° and 45°, respectively. More than two-fold improvement of dilution at the terminal and return points was achieved by the increase of inclination from 30° to 60°. This enhancement in the dilutions was 39% and 20% for the terminal and return points, respectively, with the changes of discharge angle from 45° to 60°. This study also questioned the insensitivity of dilution performance to the nozzle discharge angles which were reported for the inclination range of about 40°-70° in the studies targeted the situation of dense jets releasing into quiescent ambient waters. As a result, this assumption cannot be a valid scenario when the dense jet interacting with the dynamic ambient waters.

Study of the jet widening results also showed that applying larger $u_r F$ values and steeper inclinations resulted in less confined and more dispersed jets. It led to the higher available surface for interacting with ambient flows and thus higher dilution rates. Variance of concentration demonstrated higher variance level when dealing with the jet discharge in the

ambient current with larger $u_r F$ magnitudes. This revealed more signs of jet and ambient water interactions and more entrainment of ambient water into the jet.

Hence, it is recommended to discharge dense effluents in the regions with higher values of ambient flow velocities or to employ lower nozzle diameters for an efficient release if the regular current regime is dictated. Deploying the jet of 60° compared to the 45° and 30° is also preferable in terms of better mixing in the dynamic waters. The findings of this investigation can be useful for the application of outfalls in the shoreline regions where less discharge inclinations are required. Finally, by applying the detailed laboratory experiments, this study attempted to provide valuable insights into the efficient design of buoyant discharges of brine effluents into dynamic ambient environments for increasing dilution.

5 References

[1] J. Kucera, Desalination: water from water, 2nd Edition, John Wiley and Sons Inc., 2019. https://doi.org/10.1002/9781119407874.

[2] T.M. Missimer, B. Jones, R.G. Maliva, Intakes and Outfalls for Seawater Reverse-Osmosis Desalination Facilities: Innovations and Environmental Impacts, Springer, New York, 2015. https://doi.org/10.1007/978-3-319-13203-7.

[3] U. Caldera, C.Breyer.-W.R. Research, undefined 2017, Learning curve for seawater reverse osmosis desalination plants: capital cost trend of the past, present, and future, Wiley Online Library. 53 (2017) 10523–10538. https://doi.org/10.1002/2017WR021402.

[4] S. Lattemann, M.D. Kennedy, J.C. Schippers, G. Amy, Chapter 2 Global Desalination Situation, Sustainability Science and Engineering. 2 (2010) 7–39. https://doi.org/10.1016/S1871-2711(09)00202-5.

[5] M.J. Baum, B. Gibbes, A. Grinham, S. Albert, P. Fisher, D. Gale, Near-Field Observations of an Offshore Multiport Brine Diffuser under Various Operating Conditions, Journal of Hydraulic Engineering. 144 (2018) 05018007. https://doi.org/10.1061/(ASCE)HY.1943-7900.0001524.

[6] P. Palomar, I.J. Losada, Desalination in Spain: Recent developments and recommendations, Desalination. 255 (2010) 97–106. https://doi.org/10.1016/J.DESAL.2010.01.008.

[7] R. Einav, F. Lokiec, Environmental aspects of a desalination plant in Ashkelon, Desalination. 156 (2003) 79–85. https://doi.org/10.1016/S0011-9164(03)00328-X.

[8] M. Taherian, S.A.R. Saeidi Hosseini, A. Mohammadian, Overview of Outfall Discharge Modeling with a Focus on Turbulence Modeling Approaches, in: Forum for Interdisciplinary Mathematics, Springer, 2022: pp. 139–177. https://doi.org/10.1007/978-981-19-1438-6_4.

[9] P. Palomar, J.L. Lara, I.J. Losada, Near field brine discharge modeling part 2: Validation of commercial tools, Desalination. 290 (2012) 28–42. https://doi.org/10.1016/j.desal.2011.10.021.

[10] S.A.R. Saeidi Hossieni, A. Mohammadian, P.J.W. Roberts, O. Abessi, Numerical Study on the Effect of Port Orientation on Multiple Inclined Dense Jets, J Mar Sci Eng. 10 (2022). https://doi.org/10.3390/jmse10050590.

[11] S. Jenkins, J. Paduan, P.J.W. Roberts, D. Schlenk, J. Weis, Management of brine discharges to coastal waters recommendations of a science advisory panel (Tech. Report No. 694), Southern California Coastal Water Research Project, Costa Mesa, CA, USA, 2012.

[12] O. Abessi, Brine Disposal and Management-Planning, Design, and Implementation, in: Veera Gnaneswar Gude (Ed.), Sustainable Desalination Handbook: Plant Selection, Design and Implementation, Elsevier Inc., 2018: pp. 259–303. https://doi.org/10.1016/B978-0-12-809240-8.00007-1.

[13] P.J.W. Roberts, A. Ferrier, G. Daviero, Mixing in Inclined Dense Jets, Journal of Hydraulic Engineering. 123 (1997) 693–699. https://doi.org/10.1061/(asce)0733-9429(1997)123:8(693).

[14] E. Gungor, P.J.W. Roberts, Experimental studies on vertical dense jets in a flowing current, Journal of Hydraulic Engineering. 135 (2009) 935–948. https://doi.org/10.1061/(ASCE)HY.1943-7900.0000106.

[15] A. Ramakanth, M.J. Davidson, R.I. Nokes, Laboratory study to quantify lower boundary influences on desalination discharges, Desalination. 529 (2022). https://doi.org/10.1016/j.desal.2022.115641.

[16] O. Abessi, P.J.W. Roberts, Effect of Nozzle Orientation on Dense Jets in Stagnant Environments, Journal of Hydraulic Engineering. 141 (2015) 06015009. https://doi.org/10.1061/(asce)hy.1943-7900.0001032.

[17] I.G. Papakonstantis, E.I. Tsatsara, Mixing Characteristics of Inclined Turbulent Dense Jets, Environmental Processes. 6 (2019) 525–541. https://doi.org/10.1007/s40710-019-00359-w.

[18] O. Abessi, P.J.W. Roberts, Dense jet discharges in shallow water, Journal of Hydraulic Engineering. 142 (2016) 1–13. https://doi.org/10.1061/(ASCE)HY.1943-7900.0001057.

[19] H. Kheirkhah Gildeh, A. Mohammadian, I. Nistor, Inclined dense effluent discharge modelling in shallow waters, Environmental Fluid Mechanics. 21 (2021) 955–987. https://doi.org/10.1007/s10652-021-09805-6.

[20] M. Taherian, A. Mohammadian, Buoyant jets in cross-flows: Review, developments, and applications, J Mar Sci Eng. 9 (2021). https://doi.org/10.3390/jmse9010061.

[21] A. Galeshi, O. Abessi, M. Yousefifard, A. Rahmani Firoozjaee, Inclined dense discharge in stagnant and wave environments: An experimental and numerical study, Ocean Engineering. 278 (2023) 114045. https://doi.org/10.1016/J.OCEANENG.2023.114045.

[22] M.A. Zeitoun, W.F. McIlhenny, R.O. Reid, C.-M. Wong, W.F. Savage, W.W. Rinne, C.L. Gransee, Conceptual designs of outfall systems for desalting plants, Research and Development Progress Rep. 550, Office of Saline Water, Washington DC, USA, 1970. http://hdl.handle.net/2027/mdp.39015078505149 (accessed October 26, 2020).

[23] G.A. Kikkert, M.J. Davidson, R.I. Nokes, Inclined Negatively Buoyant Discharges, Journal of Hydraulic Engineering. 133 (2007) 545–554. https://doi.org/10.1061/(asce)0733-9429(2007)133:5(545).

[24] G.H. Jirka, Improved discharge configurations for brine effluents from desalination plants, Journal of Hydraulic Engineering. 134 (2008) 116–120. https://doi.org/10.1061/(ASCE)0733-9429(2008)134:1(116).

[25] I.G. Papakonstantis, G.C. Christodoulou, P.N. Papanicolaou, Inclined negatively buoyant jets 1: Geometrical characteristics, Journal of Hydraulic Research. 49 (2011) 3–12. https://doi.org/10.1080/00221686.2010.537153.

[26] I.G. Papakonstantis, G.C. Christodoulou, P.N. Papanicolaou, Inclined negatively buoyant jets 2: Concentration measurements, Journal of Hydraulic Research. 49 (2011) 13–22. https://doi.org/10.1080/00221686.2010.542617.

[27] C.C.K. Lai, J.H.W. Lee, Mixing of inclined dense jets in stationary ambient, Journal of Hydro-Environment Research. 6 (2012) 9–28. https://doi.org/10.1016/j.jher.2011.08.003.

[28] C.J. Oliver, M.J. Davidson, R.I. Nokes, Predicting the near-field mixing of desalination discharges in a stationary environment, Desalination. 309 (2013) 148–155. https://doi.org/10.1016/j.desal.2012.09.031.

[29] S. Ferrari, M.G. Badas, G. Querzoli, On the effect of regularwaves on inclined negatively buoyant jets, Water (Switzerland). 10 (2018). https://doi.org/10.3390/w10060726.

[30] J. Chang, Y. Du, X. Shao, Y. Zhao, S. Zheng, Investigation and analysis of vortex and application of jet in crossflow, Case Studies in Thermal Engineering. 14 (2019) 0–6. https://doi.org/10.1016/j.csite.2019.100459.

[31] M.J. Baum, B. Gibbes, Field-Scale Numerical Modeling of a Dense Multiport Diffuser Outfall in Crossflow, Journal of Hydraulic Engineering. 146 (2020) 1–16. https://doi.org/10.1061/(ASCE)HY.1943-7900.0001635.

[32] S.S. Tong, K.D. Stolzenbaeh, Submerged Discharges of Dense Effluent: Report No. 243, Massachusetts Institute of Technology, Cambridge, Massachussetts, USA, 1979. https://repository.tudelft.nl/islandora/object/uuid%3A397fe811-d155-430c-83ad-735073f07dc6 (accessed October 26, 2020).

[33] P.J.W. Roberts, G. Toms, Inclined Dense Jets in Flowing Current, Journal of Hydraulic Engineering. 113 (1987) 323–340. https://doi.org/10.1061/(asce)0733-9429(1987)113:3(323).

[34] W.R. Lindberg, Experiments on Negatively Buoyant Jets, with and without Cross-Flow, Recent Research Advances in the Fluid Mechanics of Turbulent Jets and Plumes. (1994) 131–145. https://doi.org/10.1007/978-94-011-0918-5_8.

[35] M. Ben Meftah, M. Mossa, Turbulence measurement of vertical dense jets in crossflow, Water (Basel). 10 (2018) 286. https://doi.org/10.3390/w10030286.

[36] M. Ben Meftah, D. Malcangio, F. De Serio, M. Mossa, Vertical dense jet in flowing current, Environmental Fluid Mechanics. 18 (2018) 75–96. https://doi.org/10.1007/s10652-017-9515-2.

[37] C.C.K. Lai, J.H.W. Lee, Initial mixing of inclined dense jet in perpendicular crossflow, Environmental Fluid Mechanics. 14 (2014) 25–49. https://doi.org/10.1007/s10652-013-9290-7.

[38] M. Jiang, A.W.K. Law, S. Zhang, Mixing behavior of 45° inclined dense jets in currents, Journal of Hydro-Environment Research. 18 (2018) 37–48. https://doi.org/10.1016/j.jher.2017.10.008.

[39] Baum, M. Jeffrey, Dense jet behaviour in dynamic receiving environments, The University of Queensland, 2019. https://doi.org/10.14264/UQL.2019.247.

[40] K.W. Choi, C.C.K. Lai, J.H.W. Lee, Mixing in the Intermediate Field of Dense Jets in Cross Currents, Journal of Hydraulic Engineering. 142 (2016) 04015041. https://doi.org/10.1061/(asce)hy.1943-7900.0001060.

[41] C. Oliver, Near field mixing of negatively buoyant jets, University of Canterbury, 2012. https://doi.org/10.26021/3017.

[42] L.A. Besalduch, M.G. Badas, S. Ferrari, G. Querzoli, On the near field behavior of inclined negatively buoyant jets, EPJ Web Conf. 67 (2014) 02007. https://doi.org/10.1051/EPJCONF/20146702007.

[43] S. Ferrari, G. Querzoli, Mixing and re-entrainment in a negatively buoyant jet, Journal of Hydraulic Research. 48 (2010) 632–640. https://doi.org/10.1080/00221686.2010.512778.